

## EFFICIENT IMAGE REGISTRATION FOR THE ANALYSIS OF DIFFERENT PHASES OF CONTRAST-ENHANCED LIVER CT DATA

R. Verdú<sup>1</sup>, J. Larrey<sup>1</sup>, J. Morales<sup>1\*</sup>, F. López<sup>2</sup>, V. Naranjo<sup>2</sup>, M. Alcañiz<sup>2†</sup>, R. López<sup>3</sup>

<sup>1</sup>Universidad Politécnica de Cartagena, Cartagena 30202, Spain

<sup>2</sup>Universidad Politécnica de Valencia, I3BH LabHuman, 46022 Valencia, Spain

<sup>3</sup>Unidad de Cirugía y Transplante Hepático. Hospital universitario La Fe, Valencia, Spain

### ABSTRACT

This paper describes the image registration block developed in the hepatic planner HepaPlan. The proposed method is intended to support clinical decisions about treatment of liver pathologies. The initial stage is the segmentation of the liver tissue as well as its internal structures and tumours in contrast-enhanced CT volumes. The second stage is non-rigid motion compensation due to CT data are acquired at different times, in arterial phase and venous phase. This image registration is necessary in order to fusion contrast-enhanced CT data and then to ease 3D volumetric measures, visualization of the liver and tumour, and to make comparisons with studies of the same patient at earlier times.

**Index Terms**— Variational image registration, non-rigid deformation, contrast-enhanced liver CT.

### 1. INTRODUCTION

Hepatocellular carcinoma is responsible for a large proportion of liver cancers. Nowadays it is the sixth most common cancer in the world as well as the most common cause of death among cirrhotic patients and also the third cause of death from neoplasia. The most effective treatment to alleviate this disease is liver transplantation, with good results in a high percentage of cases [1].

Currently, the specialist uses magnetic resonance imaging (MRI) or computed tomography (CT) images, in addition to their knowledge and experience, to give the diagnosis, plan the treatment, as well as to track the evolution over time of the pathology in the patient. HepaPlan is a research and development (R&D) project<sup>†</sup> which is intended to assist the physician in these three phases, providing a tool to quantitatively classify the diseases with the highest degree of objectivity while allowing a three-dimensional view of the liver structure. HepaPlan consists of a segmentation block, a registration block and a measurement block. This paper focuses on the non-rigid registration method, a constitutive block of HepaPlan.

\*This work is partially supported by *Ministerio de Ciencia e Innovación*, under grant TEC2009-12675/TEC.

<sup>†</sup>This work has been supported by the project ONCOTIC (IDI-20101153) of CDTI and Hospital Clínica Benidorm.

For many years, researchers have developed and implemented registration algorithms for medical imaging applications. In [2], non-rigid registration techniques are evaluated on thoracic CT images. Particularly, the liver segmentation is an open challenge [3], which provides an interesting setting for comparing image registration methods. A novel collection of medical image registration algorithms in C++ based on ITK [5] can be found in [4]. However, this collection restricts non-rigid transformations to *B*-spline models [6] or physical model-based splines [7], not taking into account non-parametric registration methods (i.e. the approach proposed in this paper or [8],[9]).

In this paper we analyze tri-phase 3D computed tomography datasets under contrast agent injection. The liver has arteries, hepatic veins and portal veins. This third blood vessel system drains venous blood from the entire gastrointestinal tract. 3D datasets are acquired at different times depending on the arrival time of the contrast agent in arteries, portal and hepatic veins. First, a study without contrast agent is acquired. Once the contrast agent is injected, it reaches the arteries (arterial phase), then the portal veins and next the hepatic veins (both in hepatic venous phase). Hepatic and portal veins are then visible in the hepatic venous phase.

Although the acquisition of the different phases is continuous, there is no exact correspondence between them, so they must be registered in order to show the results in a common 3D scenario. This provides objective parameters of the pathology which facilitate comparisons between patients, the tracking of tumours [10], to make calculations on the volume of the liver to be preserved prior to a liver resection [11] or to generate vessel models for planning surgical procedures [12].

In this work we track the non-rigid deformation that undergoes in the different phases of contrast-enhanced CT data of the liver. This allows to locate exactly the vessels in 3D at each phase of contrast-enhanced CT data in order to measure distances and volumes. The method is based on an efficient implementation of variational image registration, which is at least two times faster than other approaches in the spatial domain [13].

## 2. VARIATIONAL IMAGE REGISTRATION

Image registration is the process of finding out the global and local correspondence between two images, template  $T$  and reference  $R$ , of a scene in such a way that the transformed template and reference match [14]. In this application the images are 3D datasets obtained from CT studies,  $R, T : \mathbb{R}^3 \rightarrow \mathbb{R}$ , and the registration will produce a non-rigid displacement field  $\mathbf{u} : \mathbb{R}^3 \rightarrow \mathbb{R}^3$  that will make the transformed template dataset similar to the reference dataset,  $T(\mathbf{x} - \mathbf{u}(\mathbf{x})) \approx R(\mathbf{x})$ , where  $\mathbf{u}(\mathbf{x}) = (u_1(\mathbf{x}), u_2(\mathbf{x}), u_3(\mathbf{x}))^\top$  and  $\mathbf{x}$  is the spatial position  $\mathbf{x} = (x_1, x_2, x_3) \in \mathbb{R}^3$ .

The non-parametric registration can be approached in terms of the variational calculus, by defining the joint energy functional to be minimized:

$$\mathcal{J}[\mathbf{u}] = \mathcal{D}[R, T; \mathbf{u}] + \alpha \mathcal{S}[\mathbf{u}]. \quad (1)$$

The energy term  $\mathcal{D}$  measures the distance between the deformed template dataset and the reference dataset;  $\mathcal{S}$  is a penalty term which acts as a regularizer and determines the smoothness of the displacement field; and  $\alpha > 0$  weights the influence of the regularization.

The distance measure  $\mathcal{D}$  is chosen depending on the datasets to be registered. When dealing with datasets from different sources or modalities (multimodal registration), statistical-based measures are more appropriate. In this application the correlation ratio [15] has been used.

The regularization term  $\mathcal{S}$  gives the smoothness characteristics to the displacement field [8]. In our case we use the diffusion term, which is given by the energy of first order derivatives of  $\mathbf{u}$ :

$$\mathcal{S}^{\text{diff}}[\mathbf{u}] = \frac{1}{2} \sum_{l=1}^3 \int_{\mathbb{R}^3} \|\nabla u_l\|^2 dx. \quad (2)$$

As described in [9], the joint energy functional (1) can be translated into the frequency domain by means of Parseval's theorem, then  $\mathcal{J}[\mathbf{u}] = \tilde{\mathcal{J}}[\tilde{\mathbf{u}}]$ , where

$$\tilde{\mathcal{J}}[\tilde{\mathbf{u}}] = \tilde{\mathcal{D}}[\tilde{R}, \tilde{T}; \tilde{\mathbf{u}}] + \alpha \tilde{\mathcal{S}}[\tilde{\mathbf{u}}], \quad (3)$$

with  $\tilde{\mathbf{u}}(\boldsymbol{\omega}) = (\tilde{u}_1(\boldsymbol{\omega}), \tilde{u}_2(\boldsymbol{\omega}), \tilde{u}_3(\boldsymbol{\omega}))^\top$  being the frequency counterpart of the displacement field,  $\boldsymbol{\omega} = (\omega_1, \omega_2, \omega_3)$  is the three dimensional variable in the frequency domain, and where the distance measure  $\tilde{\mathcal{D}}$  and the regularization term  $\tilde{\mathcal{S}}$  are now defined in the frequency domain.

According to the variational calculus, a necessary condition for a minimizer  $\tilde{\mathbf{u}}$  of the joint energy functional (3) is that the first variation of  $\tilde{\mathcal{J}}[\tilde{\mathbf{u}}]$  in any direction (also known as the *Gâteaux* derivative) vanishes for all suitable perturbations. This leads to the Euler-Lagrange equation in the frequency domain:

$$\tilde{\mathbf{f}}(\boldsymbol{\omega}) + \alpha \tilde{\mathcal{A}}(\boldsymbol{\omega}) \tilde{\mathbf{u}}(\boldsymbol{\omega}) = \mathbf{0}, \quad (4)$$

where  $\tilde{\mathbf{f}}$  is the 3D Fourier transform of the external forces,  $\mathcal{FT}\{\nabla \mathcal{D}[R, T; \mathbf{u}]\}$ , and  $\tilde{\mathcal{A}}$  is a diagonal  $3 \times 3$  matrix whose

elements are scalar functions which implement the spatial derivatives in the frequency domain [13], allowing for their computation by means of products:

$$\tilde{\mathcal{A}}_{ii}(\boldsymbol{\omega}) = 2 \sum_{m=1}^3 (1 - \cos \omega_m). \quad (5)$$

The Euler-Lagrange equations (4) in the frequency domain provide a stable implementation for the computation of a numerical solution for the displacement field, and in a more efficient way than existing approaches if the three-dimensional fast Fourier transform is used [13]. To solve (4), formulated in the frequency domain, a time-marching scheme can be employed, yielding the following equation:

$$\partial_t \tilde{\mathbf{u}}(\boldsymbol{\omega}, t) + \tilde{\mathbf{f}}(\boldsymbol{\omega}, t) + \alpha \tilde{\mathcal{A}}(\boldsymbol{\omega}) \tilde{\mathbf{u}}(\boldsymbol{\omega}, t) = \mathbf{0}, \quad (6)$$

where  $\partial_t \tilde{\mathbf{u}}(\boldsymbol{\omega}, t) = (\partial_t \tilde{u}_1(\boldsymbol{\omega}, t), \partial_t \tilde{u}_2(\boldsymbol{\omega}, t), \partial_t \tilde{u}_3(\boldsymbol{\omega}, t))^\top$  (in the steady-state  $\partial_t \tilde{\mathbf{u}}(\boldsymbol{\omega}, t) = \mathbf{0}$  and (6) holds (4)). Equation (6) is solved by discretizing the time,  $t = \xi\tau$ ,  $\tau > 0$  being the time-step and  $\xi \in \mathbb{N}$  being the iteration index, and the time derivative of  $\tilde{\mathbf{u}}(\boldsymbol{\omega}, t)$  is replaced by the first backward difference. Using the notation  $\tilde{\mathbf{u}}^{(\xi)}(\boldsymbol{\omega}) = \tilde{\mathbf{u}}(\boldsymbol{\omega}, \xi\tau)$ , the following semi-implicit iterative scheme comes out:

$$\tilde{u}_l^{(\xi)}(\boldsymbol{\omega}) = H(\boldsymbol{\omega}) (\tilde{u}_l^{(\xi-1)}(\boldsymbol{\omega}) - \eta^{-1} \tilde{f}_l^{(\xi-1)}(\boldsymbol{\omega})), \quad (7)$$

where  $l = \{1, 2, 3\}$ ,  $\eta = 1/\tau$  and  $H(\boldsymbol{\omega})$  is the following 3D low pass filter  $H(\boldsymbol{\omega}) = (1 + \eta^{-1} \alpha \tilde{\mathcal{A}}_{ii}(\boldsymbol{\omega}))^{-1}$ . An implementation based on the 3D FFT is, in terms of efficiency, two times faster than the fastest implementation available in the spatial domain [13], which is the DCT-based algorithm included in the FLIRT toolbox [16] for the diffusion and curvature registration methods [17].

## 3. RESULTS

This section shows the non-rigid alignment of different phases of contrast-enhanced liver 3D CT data acquired at two different times. The studies were obtained using a Toshiba Aquilion scanner and a Philips Brilliance 64 scanner, and then reformatted into DICOM files of different resolutions. For all experiments shown in this work, the registration parameters are the same:  $\alpha = 10$ ,  $\eta = 1$  and  $\xi_{max} = 50$ . With these parameters, the optimal performance of the algorithm is achieved, obtaining at the same time a likely and smooth transformation. The diffusion regularizer  $\mathcal{S}^{\text{diff}}$  ensures a correct outcome in this scenario, since it privileges translations (which can be clearly appreciated in the second and third experiment) in the computed displacement field  $\mathbf{u}$  [17].

Fig.1 displays the registration of two scans corresponding to the arterial phase (reference dataset,  $R$ ) and the portal phase (template dataset,  $T$ ) of the same patient. In this case, the volumes to be registered are initially almost geometrically aligned. This fact can be noticed by visual inspection

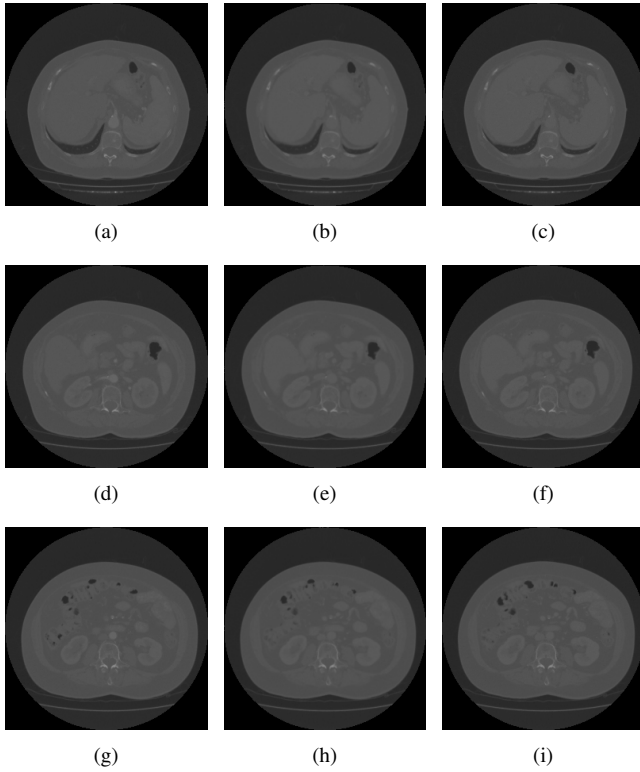


**Fig. 1.** Experiment 1: registration of the arterial phase and the portal phase of the same patient ( $256 \times 256 \times 75$  voxels). First column: reference dataset. Second column: registered template. Third column: template dataset. First row: slice #28. Second row: slice #46. Third row: slice #56.

of the first and third columns of Fig.1. Indeed, the similarity measurements (gathered in Table 1) are particularly high for this experiment: the *peak signal-to-noise ratio* (PSNR) before registration is over 40 dB (it should be noted that a PSNR higher than 27 – 30 dB is usually considered in image registration literature as a good match), while the *correlation ratio* (CR) is over 99% (where a value of 100% means a perfect match). Nevertheless, as can be seen in the second column of Fig.1 and also in the first column of Table 1, the proposed registration procedure can improve the alignment of the datasets even in this (almost) trivial scenario.

In the second experiment (Fig.2) the aim is to register two volumetric scans corresponding to the non-contrast phase (reference dataset,  $R$ ) and the arterial phase (template dataset,  $T$ ) of the same patient. If we compare the first and third columns of Fig.2, an overall translational misalignment can be easily observed. Moreover, there exist slight non-rigid differences between the two datasets that have to be also corrected, therefore the proposed regularization term is particularly suitable for this scenario. After the registration process (shown in the second column of Fig.2), the computed PSNR and CR measurements are over 30 dB and 99%, respectively.

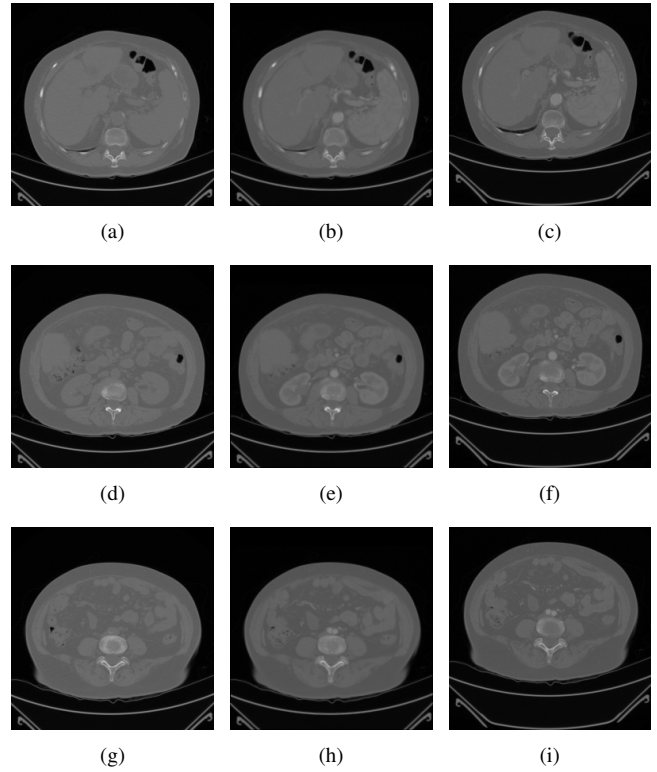


**Fig. 2.** Experiment 2: registration of the non-contrast phase and the arterial phase of the same patient ( $256 \times 256 \times 79$  voxels). First column: reference dataset. Second column: registered template. Third column: template dataset. First row: slice #28. Second row: slice #46. Third row: slice #68.

Please note that the initial values of these similarity measures were very low, hence we can conclude that our approach provides satisfactory results.

**Table 1.** Similarity measures computed for the experiments.

	Fig.1	Fig.2	Fig.3
PSNR before registration	40.53 dB	15.72 dB	15.59 dB
PSNR after registration	43.31 dB	31.39 dB	27.28 dB
CR before registration	99.52%	37.84%	32.74%
CR after registration	99.77%	99.21%	96.76%

The last experiment, displayed in Fig.3, constitutes the most difficult registration scenario amongst the three presented in this paper. Both reference ( $R$ , see first column of Fig.3) and template ( $T$ , see third column of Fig.3) datasets correspond to the arterial phase of the same patient, but they were acquired with different scanners at two different times (more precisely,  $R$  was acquired three months later than  $T$ ). The outcome of the proposed registration algorithm is shown in the second column of Fig.3. The measured PSNR and CR are gathered in Table 1. Although in this case the registration

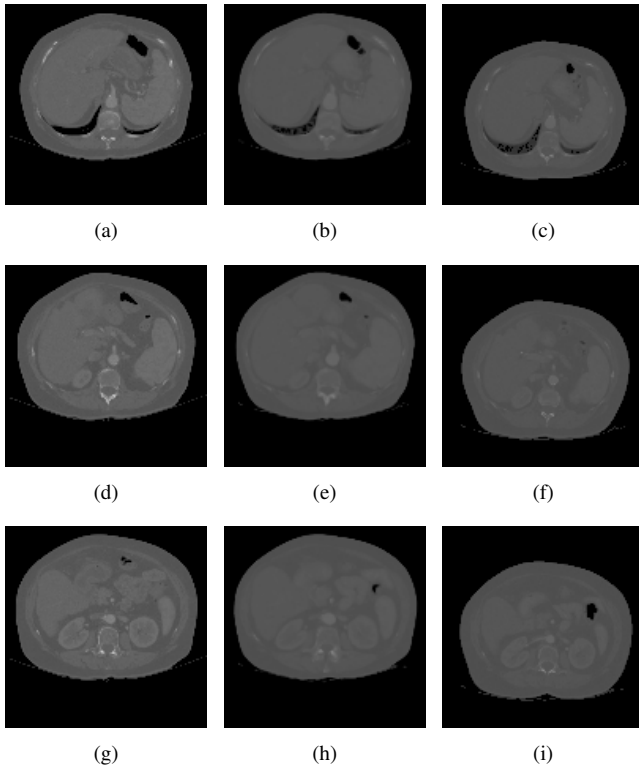


**Fig. 3.** Experiment 3: registration of the arterial phase of the same patient, acquired at two different times ( $256 \times 256 \times 67$  voxels). First column: reference dataset. Second column: registered template. Third column: template dataset. First row: slice #25. Second row: slice #34. Third row: slice #42.

result is far from perfect (visually nor numerically), it can be considered good enough, since the initial datasets differ significantly (which contributes to the inherent ill-posedness of the registration problem).

#### 4. CONCLUSIONS

This paper addresses an efficient implementation of variational image registration of contrast-enhanced liver CT data. The method is based on an efficient implementation of the diffusion registration in the frequency domain. Results on different phases of contrast-enhanced liver CT data show the ability and high accuracy of the proposed method to estimate the deformation existing in these 3D acquisitions.

The authors are working on the implementation of this method in C++ using ITK in order to compare it to other methods and this way prove its efficiency.

#### 5. REFERENCES

[1] V. Mazzaferro *et al.*, “Liver transplantation for the treatment of small hepatocellular carcinomas in patients with cirrhosis,”

*New England J Medicine*, vol. 334, 1996.

- [2] K. Murphy *et al.*, “Evaluation of registration methods on thoracic CT: The EMPIRE10 challenge,” *IEEE Trans. Medical Imaging*, vol. 30, no. 11, pp. 1901–1920, 2011.
- [3] T. Heimann *et al.*, “Comparison and evaluation of methods for liver segmentation from CT datasets,” *IEEE Trans. Medical Imaging*, vol. 28, pp. 1251–1265, 2009.
- [4] S. Klein *et al.*, “elastix: A toolbox for intensity-based medical image registration,” *IEEE Trans. Medical Imaging*, vol. 29, no. 1, pp. 196–205, 2010.
- [5] L. Ibáñez, W. Schroeder, L. Ng, and J. Cates, *The ITK Software Guide*, Kitware, Clifton Park, NY, 2005.
- [6] D. Rueckert *et al.*, “Nonrigid registration using free-form deformations: application to breast MR images,” *IEEE Trans. Med. Imaging*, vol.18, pp.712–721, 1999.
- [7] M.H. Davis *et al.*, “A physics-based coordinate transformation for 3D image matching,” *IEEE Trans. Medical Imaging*, vol. 16, no. 3, pp. 317–328, 1997.
- [8] B. Fischer and J. Modersitzki, “A unified approach to fast image registration and a new curvature based registration technique,” *Linear Algebra & its Applications*, vol. 308, 2004.
- [9] J. Larrey-Ruiz, R. Verdú-Monedero, and J. Morales-Sánchez, “A Fourier domain framework for variational image registration,” *J. Math. Imaging Vis.*, vol. 32, no. 1, pp. 57–72, 2008.
- [10] A. Charnoz *et al.*, “Liver registration for the follow-up of hepatic tumors,” in *Medical Image Computing and Computer-Assisted Intervention MICCAI*, vol. 3750. LNCS, 2005.
- [11] H. Elhawary *et al.*, “Intra-operative multimodal non-rigid registration of the liver for navigated tumor ablation,” in *MICCAI*, vol. 5761, LNCS Springer, 2009.
- [12] T. Lange *et al.*, “Registration of different phases of contrast-enhanced ct/mri data for computer-assisted liver surgery planning: Evaluation of state-of-the-art methods,” *The Int. J. Medical Robotics & Computer Assisted Surgery*, vol. 1, 2005.
- [13] R. Verdu-Monedero, J. Larrey-Ruiz, and J. Morales-Sanchez, “Frequency implementation of the Euler-Lagrange equations for variational image registration,” *Signal Processing Letters, IEEE*, vol. 15, pp. 321–324, 2008.
- [14] B. Zitová and J. Flusser, “Image registration methods: a survey,” *Image and Vision Computing*, vol. 21, 2003.
- [15] A. Roche, G. Malandain, X. Pennec, and N. Ayache, “The correlation ratio as a new similarity measure for multimodal image registration,” in *MICCAI*, vol. 1496. LNCS, 1998.
- [16] B. Fischer and J. Modersitzki, “Flirt: A flexible image registration toolbox,” *Biomedical Image Registration*, vol. 2717, LNCS Springer, 2003.
- [17] Jan Modersitzki, *Numerical Methods for Image Registration*, Oxford University Press, USA, 2004.